Domain decomposition preconditioners for multiscale problems

Yalchin Efendiev* Juan Galvis†

Abstract

In this paper, we study domain decomposition preconditioners for multiscale elliptic problems in high contrast media. We construct preconditioners such that the condition number of the preconditioned system is independent of media contrast. For this purpose, multiscale spaces for the interpolation on the coarse grid is developed using a local weighted spectral problem. A main observation is that the eigenvalues of this spectral problem control the condition number. In the presence of high-contrast inclusions, there are small, asymptotically vanishing, eigenvalues, i.e., these eigenvalues decrease as we increase the contrast. We propose the coarse space that includes the eigenfunctions corresponding to these small, asymptotically vanishing, eigenvalues. We prove that domain decomposition preconditioners with this coarse space result to the convergence of the methods independent of the contrast. The coarse space constructed using the eigenfunctions of local spectral problem can be large if there are many isolated inclusions. We propose approaches to reduce the dimension of the coarse space. Numerical results are presented. We compare the proposed methods with domain decomposition methods where multiscale finite element basis or energy minimizing basis functions are used in constructing coarse spaces. We show that the number of iterations is smaller with proposed methods and they remain bounded as the contrast increases.

1 Introduction

Many processes occur in a multiscale environment that have high variations in the media properties. For example, subsurface flows are often affected by heterogeneities in a wide range of length scales and the media properties often vary significantly in short distances. A high contrast in the media properties brings an additional small scale into the problem expressed as the ratio between

*Department of Mathematics, Texas A & M University, College Station, TX 77843 (efendiev@math.tamu.edu)

†Department of Mathematics, Texas A & M University, College Station, TX 77843 (jugal@math.tamu.edu). Corresponding author.

low and high conductivity values. In fact, there may not be a distinct small scale in the media properties. For example, it is common to have several orders of magnitude of variations or even continuous variations in the permeability values in natural porous formations. Moreover, low or high conductivity regions can have complex geometry that can introduce connected regions at different scales.

In this paper we investigate domain decomposition preconditioners for flows in heterogeneous porous media. Domain decomposition methods use the solutions of small local and coarse problems in constructing preconditioners for the fine-scale system. The number of iterations required by domain decomposition preconditioners is typically affected by the contrast in the media properties that are within each coarse grid block. It is known that if high and low conductivity regions can be encompassed within coarse grid blocks such that the variation of the conductivity within each coarse region is bounded, domain decomposition preconditioners result to a system with the condition number independent of the contrast (e.g., [18, 23]). Because of complex geometry of fine-scale features, it is often impossible to separate low and high conductivity regions into different coarse grid blocks. E.g., low or high conductivity regions can have small sizes in the shape of narrow channels. Encompassing these regions into coarse grids can make the computations difficult because these regions are often difficult to identify due to changes in geometry, the sizes and conductivity variations within them. Design of domain decomposition preconditioners when coarse grids contain high media variability remains a challenging problem.

When the conductivity field varies significantly within each coarse-grid block, domain decomposition methods may not yield preconditioners with bounded (independent of the contrast) condition number. In a recent pioneering work [15, 16], it has been shown that using domain decomposition methods, one can precondition the fine-scale system such that the condition number of the resulting preconditioned system is independent of the contrast when high conductivity inclusions are embedded into the media of bounded conductivity. The approach presented in [15] is not applicable to the general case considered in this paper where we construct domain decomposition methods that result to preconditioners with bounded (independent of the contrast) condition number.

The main idea of our work consists of modifying the coarse space that appears in the formulation of domain decomposition methods. We introduce a coarse space based on local spectral problems. These spaces are motivated by weighted Poincaré estimates that arise in the proofs of L^2 approximation property of the coarse interpolation in the analysis of domain decomposition preconditioners. In particular, weighted Poincaré estimates suggest to use a particular eigenvalue problem that is considered in this paper. It can be shown in the presence of high-contrast inclusions this eigenvalue problem detects the basis functions that are needed in the coarse space. These basis functions are the eigenfunctions that correspond to the small, asymptotically vanishing, eigenvalues. We prove that if the coarse space in domain decomposition methods includes these eigenfunctions, then the condition number of the preconditioned matrix is bounded independent of the contrast. We use partition of unity functions to span the eigenfunctions. Our construction of the coarse space automat-

ically selects appropriate basis elements independent of the geometry or scale separation in the problem.

The coarse space constructed using the eigenfunctions of the weighted spectral problem can be large, in general. This is because the weighted eigenvalue problem detects every isolated inclusion and channel. Consequently, if the number of inclusions and channels is large, then the dimension of the coarse space also becomes large. In this paper, we discuss the dimension reduction for the coarse space. We first propose an energy minimizing space for our local spectral multiscale space. Then we consider the energies of the obtained basis functions. The energies of the basis functions that correspond to the inclusions are bounded independent of the contrast. We propose a procedure that selects these basis functions and they are replaced by nodal multiscale finite element basis functions.

In this paper, we study two level additive Schwartz preconditioners with several coarse solvers. In the overlapping setting, since we would like to treat heterogeneous media, we concentrate on the case of generous and big overlap. In this case the size of the overlap is of the order of the size of the coarse triangulation parameter. Numerical results are presented to show that the condition number of the preconditioned system is independent of the contrast. In particular, we implement an approach where an arbitrary number of basis functions per node can be chosen. For the coarse solvers, we consider various choices for basis functions - piecewise linear basis, multiscale finite element basis functions, energy minimizing basis functions, and new coarse spaces obtained using the solutions of local weighted eigenvalue problem. We show that using new spectral coarse spaces one achieves less number of iterations and moreover, the condition number is bounded in contrast when other coarse spaces are used. Furthermore, we show that one can reduce the number of basis functions and domain decomposition preconditioners with reduced number of basis functions behave similar to the ones without any reduction. This reduction can be significant if there are many inclusions within coarse-grid blocks.

The paper is organized in the following way. In the next section, we present an outline of the results. Problem setting and domain decomposition framework are presented in Section 3. Section 4 is devoted to the high contrast eigenvalue problem setting where some key inequalities are shown. In Section 5, we present the analysis of domain decomposition methods and numerical results. In Section 6, we present an approach to reduce the energy of the basis functions and corresponding numerical results. Section 7 is devoted to the discussions on dimension reduction of the coarse space. We present an algorithm and numerical results in this section.

2 Outline of results. High-contrast eigenvalue problem and coarse spaces

Previous approaches concerning overlapping domain decomposition address the cases where the permeability fields are nearly homogeneous within each coarse-grid block (e.g., [18, 23]) or high conductivity regions constitute disconnected regions within a coarse-grid block [15, 16]. In this paper, we propose domain decompositions preconditioners such that the condition number of the preconditioned system is independent of the contrast. Our method is motivated by weighted Poincaré estimates that are needed in proving L^2 stability of the coarse projection. In particular, one needs to show that

$$\int \kappa(x)|v|^2 \leq C \int \kappa(x)|\nabla v|^2$$

for all v that have zero component in the coarse space. Here, the integral is taken over a coarse region and C is independent of the contrast $\kappa(x)$. In our previous work [14], we prove weighted Poincaré estimates for a class of heterogeneities. However, this inequality is not valid for general heterogeneities unless the coarse projection is properly chosen. The weighted Poincaré estimate suggests the use of the following zero Neumann eigenvalue problem

$$\text{div}(\kappa(x)\nabla\phi_i) = \lambda_i \kappa(x)\phi_i \tag{1}$$

in constructing the coarse-scale projection. In particular, the eigenvalue problem (1) is considered locally in the union of coarse grid blocks with a common vertex.

The problem (1) has eigenvalues that scale as the inverse of the high contrast. To demonstrate this, we plot eigenvectors for a particular case in Figure 1. There are six inclusions, two channels and four inclusions that have high conductivity. The background conductivity is one. As a result, there are six eigenvalues that are small and asymptotically vanish as the high conductivity increases. These eigenvalues are scaled as the inverse of the high contrast and the rest of eigenvalues are large and remain bounded below as the contrast increases. Assume that the eigenvalues are ordered as $\lambda_1 \leq \lambda_2 \leq ... \leq \lambda_L < \lambda_{L+1} \leq ... \leq \lambda_N$, where λ_1, ..., λ_L are small, asymptotically vanishing eigenvalues. We show that if the coarse space includes the eigenfunctions corresponding to the eigenvalues λ_1, ..., λ_L, then the condition number of the preconditioned matrix scales as $\max(1/\lambda_{L+1})$, where maximum is taken over all coarse grid blocks. This result holds in general and depends on which eigenvectors are included in the coarse space. Once the eigenfunctions corresponding to small, asymptotically vanishing, eigenvalues are selected in the coarse space, one can show that the condition number of the preconditioned system is bounded independent of the contrast. An important feature of the proposed approach is that one can choose the cut-off for the eigenvalues and control the condition number of the preconditioned system. This is particularly important for porous media applications when there is no clear separation in the contrast scales. Thus, by imposing a threshold we control the condition number of the preconditioned system. If in

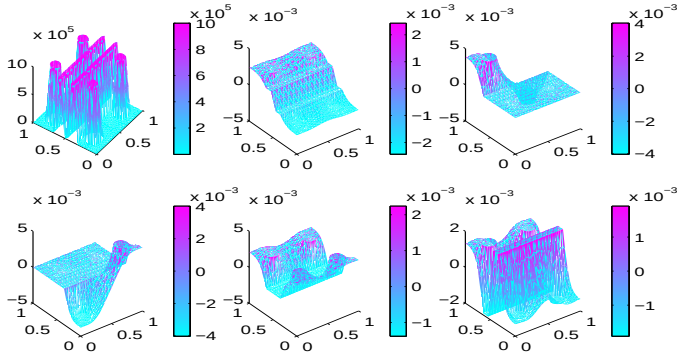

Figure 1: Eigenfunctions for Neumann problem. Permeability is 10^6 in the inclusions and channels and 1 outside. Left top: permeability. Middle top: second eigenfunction (fist eigenfunction is constant). Right top: third eigenfunction. Left bottom: fourth eigenfunction. Middle bottom: fifth eigenfunction. Right bottom: sixth eigenfunction. The six small eigenvalues are 0, $0.0873e-3$, $0.1879e-3$, $0.1879e-3$, $0.2693e-3$, and $0.3821e-3$.

the example above the inclusions have small conductivities (instead of large), then there are three small (asymptotically vanishing) eigenvalues due to the fact that the channels divide the domain into three connected regions.

In the case of many inclusions, the number of the small, asymptotically vanishing, eigenvalues can be large. In this case, the dimension of the coarse space is large (see Section 7 for numerical results). In this paper, we propose a strategy to reduce the dimension of the coarse space. We show that it is possible to reduce the dimension of the coarse space by combining the eigenfunctions that correspond to the inclusions that are strictly inside the coarse-grid block. One can identify the number of basis functions that are due to the inclusions which lie strictly inside the coarse grid block by solving Dirichlet eigenvalue problem. In Figure 2, we plot the eigenvectors for the eigenvalue problem considered above with zero Dirichlet boundary conditions (instead of Neumann). As we see that there are only four small, asymptotically vanishing, eigenvalues. In this case, the channels do not enter in the eigenfunctions because of zero Dirichlet boundary conditions. We can conclude from here that there are only two eigenfunctions that represent channels. Thus, Dirichlet problem helps us to identify the number of interior high-contrast inclusions. In general case, it is difficult to separate eigenfunctions corresponding to channels that intersect the boundary of a coarse block from those corresponding to inclusions. To identify the eigenvectors that correspond to channels, we introduce local spectral energy minimizing basis functions that have the least energy and span the eigenfunctions corresponding to small, asymptotically vanishing, eigenvalues.

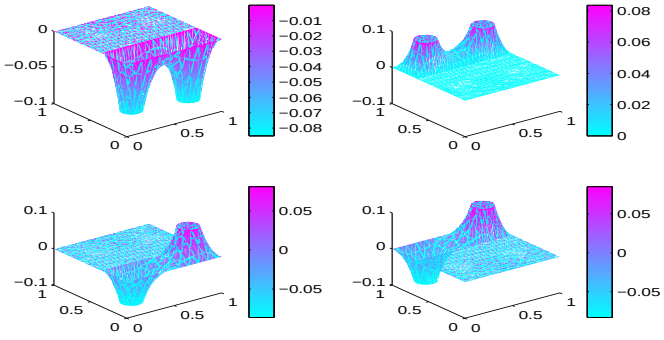

Figure 2: Eigenfunctions for Dirichlet problem with the same permeability as in Figure 1. Left top: first eigenfunction. Right top: second eigenfunction. Left bottom: third eigenfunction. Right bottom: fourth eigenfunction. The four small eigenvalues are $0.2894e-3$, $0.2895e-3$, $0.2946e-3$, and $0.2947e-3$.

3 Problem Setting and domain decomposition framework

Let $D \subset \mathbb{R}^2$ (or $\mathbb{R}^3$) be a polygonal domain which is the union of a disjoint polygonal subregions $\{D_i\}_{i=1}^N$. We consider the following problem. Find $u^* \in H_0^1(D)$ such that

$$a(u^*, v) = f(v) \quad \text{for all } v \in H_0^1(D). \tag{2}$$

Here the bilinear form a and the linear functional f are defined by

$$a(u, v) = \int_D \kappa(x) \nabla u(x) \nabla v(x) dx \quad \text{for all } u, v \in H_0^1(D) \tag{3}$$

and

$$f(v) = \int_D f(x) v(x) dx \quad \text{for all } v \in H_0^1(D).$$

We assume that the decomposition $\{D_i\}_{i=1}^N$ form a quasiuniform triangulation of D with parameter $H = \max_i \operatorname{diam}(D_i)$. This coarse triangulation will be also denoted by $\mathcal{T}^H$. Let $\mathcal{T}^h$ be a fine triangulation which is a refinement of $\mathcal{T}^H$.

We denote by $V^h(D)$ the usual finite element discretization of piecewise linear continuous functions with respect to the fine triangulation $\mathcal{T}^h$. Denote also by $V_0^h(D)$ the subset of $V^h(D)$ with vanishing values on ∂D. Similar notations, $V^h(\Omega)$ and $V_0^h(\Omega)$, are used for subdomains $\Omega \subset D$.

The Galerkin formulation of (2) is to find $u^* \in V_0^h(D)$ such that

$$a(u^*, v) = f(v) \quad \text{for all } v \in V_0^h(D), \tag{4}$$

or in matrix form

$$Au^* = b \tag{5}$$

where for all $u, v \in V^h(D)$ we have

$$u^T Av = \int_D \kappa \nabla u \nabla v \quad \text{and} \quad v^T b = \int_D fv.$$

Remark 1 *It is enough to consider the case of piecewise constant coefficient κ with respect to the fine-scale triangulation $\mathcal{T}^h$. From now on we will assume that κ is piecewise constant coefficient with value $\kappa = \kappa_e$ on each fine triangulation element $e \in \mathcal{T}^h$.*

We denote by $\{D_i'\}_{i=1}^N$ the overlapping decomposition obtained from the original nonoverlapping decomposition $\{D_i\}_{i=1}^N$ by enlarging each subdomain D_i to

$$D_i' = D_i \cup \{x \in D, \text{dist}(x, D_i) < \delta_i\}, \quad i = 1, \ldots, N,$$

where dist is some distance function and $\delta = \max_{1 \le i \le N} \delta_i$. Let $V_0^i(D_i')$ be the set of finite element functions with support in D_i'. We also denote by $R_i^T : V_0^i(D_i') \to V^h$ the extension by zero operator.

Using the coarse interpolation $\mathcal{T}^H$ we introduce coarse basis functions $\{\Phi_i\}_{i=1}^{N_c}$ where N_c is the number of coarse mesh vertices. In the general setting of domain decomposition solvers the coarse triangulation may be independent of the subdomain partition of the original domain D. Here, in order to simplify the analysis we have assumed that the coarse triangulation coincides with the nonoverlapping decomposition.

Given coarse-scale basis functions $\{\Phi_i\}_{i=1}^{N_c}$ we define the coarse space by

$$V_0 = \text{span}\{\Phi_i\}_{i=1}^{N_c}, \tag{6}$$

and the coarse matrix $A_0 = R_0 A R_0^T$ where

$$R_0^T = [\Phi_1, \ldots, \Phi_{N_c}].$$

We use a two level additive preconditioner of the form

$$B^{-1} = R_0^T A_0^{-1} R_0 + \sum_{i=1}^N R_i^T A_i^{-1} R_i \tag{7}$$

where the local matrices are defined by

$$vA_i w = a(v, w) \quad \text{for all } v, w \in V^i = V_0^h(D_i'), \tag{8}$$

$i = 1, \ldots, N$. See [23, 18].

We denote by $\{y_i\}_{i=1}^{N_c}$ the vertices of the coarse mesh $\mathcal{T}^H$ and define the neighborhood of the node y_i by

$$\omega_i = \bigcup \{K \in \mathcal{T}^H; \quad y_i \in \overline{K}\} \tag{9}$$

and the neighborhood of the coarse element K by

$$\omega_K = \bigcup \{\omega_j; \quad y_j \in \overline{K}\}. \tag{10}$$

Throughout, $a \preceq b$ means that $a \leq Cb$ where the constant C is independent of the mesh size and contrast.

4 Main tools. Stability estimates

In this section we define the new local spectral multiscale coarse space using eigenvectors of high contrast eigenvalue problems. Fist we introduce the notations for the eigenvalues problem.

For any $\Omega \subset D$ define the Neumann matrix A^Ω by

$$v^T A^\Omega w = \int_\Omega \kappa \nabla v \nabla w \quad \text{for all } v, w \in \widetilde{V}^h(\Omega), \tag{11}$$

and the mass matrix of same dimension M^Ω by

$$v^T M^\Omega w = \int_\Omega \kappa v w \quad \text{for all } v, w \in \widetilde{V}^h(\Omega). \tag{12}$$

where $\widetilde{V}_h = V_h(\Omega)$ if $\overline{\Omega} \cap \partial D = \emptyset$ and $\widetilde{V}_h = \{v \in V_h(\Omega) : v = 0 \text{ on } \partial\Omega \cap \partial D\}$ otherwise. We consider the finite dimensional symmetric eigenvalue problem

$$A^\Omega \phi = \lambda M^\Omega \phi \tag{13}$$

and denote its eigenvalues and eigenvectors by $\{\lambda_\ell^\Omega\}$ and $\{\psi_\ell^\Omega\}$, respectively. Note that the eigenvectors $\{\psi_\ell^\Omega\}$ form an orthonormal basis of $V^h(\Omega)$ with respect to the M^Ω inner product. Assume that

$$\lambda_1^\Omega \leq \lambda_2^\Omega \leq \ldots \leq \lambda_i^\Omega \leq \ldots, \tag{14}$$

and note that $\lambda_1^\Omega = 0$. The eigenvalue problem above corresponds to the approximation of the eigenvalue problem

$$\operatorname{div}(\kappa \nabla u) = \lambda \kappa u$$

in Ω with Neumann boundary condition. In particular, $\psi_\ell^{\omega_i}$ denotes the ℓ-th eigenvector of the Neumann matrix associated to the neighborhood of y_i. In Section 2, we showed an example case, where there are four high-conductivity inclusions and two high-conductivity channels. As we observed there are six

small, asymptotically vanishing, eigenvalues (see Figures 1 and 2). In general, if there are n inclusions and channels, then one can observe n small, asymptotically vanishing, eigenvalues. The eigenvectors corresponding to these eigenvalues will be used to construct the coarse space V_0. We note that for the proposed methods, we only need to specify the eigenvectors based on the quantities $\{1/\lambda_l^{\omega_i}\}$ in each ω_i. These eigenvectors are used to construct the coarse space.

We assume that the elements of $\mathcal{T}^h$ contained in Ω form a triangulation of Ω. Let $n_h(\Omega)$ denote the number of degrees of freedom in $\overline{\Omega}$. Given any $v \in V^h(\Omega)$ we can write

$$v = \sum_{\ell=1}^{n_h(\Omega)} \left(v^T M^\Omega \psi_\ell^\Omega\right) \psi_\ell^\Omega = \sum_{\ell=1}^{n_h(\Omega)} \left(\int_\Omega \kappa v \psi_\ell^\Omega\right) \psi_\ell^\Omega$$

and compute

$$\int_\Omega \kappa |\nabla v|^2 = v^T A^\Omega v = \sum_{\ell=1}^{n_h(\Omega)} \left(\int_\Omega \kappa v \psi_\ell^\Omega\right)^2 \lambda_\ell^\Omega \tag{15}$$

and

$$\int_\Omega \kappa v^2 = v^T M^\Omega v = \sum_{\ell=1}^{n_h(\Omega)} \left(\int_\Omega \kappa v \psi_\ell^\Omega\right)^2. \tag{16}$$

Given an integer L and $v \in V^h(\Omega)$ define

$$I_L^\Omega v = \sum_{\ell=1}^{L} \left(\int_\Omega \kappa v \psi_\ell^\Omega\right) \psi_\ell^\Omega. \tag{17}$$

From (14), (15), and (16) it is easy to prove the following inequality

$$\int_\Omega \kappa (v - I_L^\Omega v)^2 \leq \frac{1}{\lambda_{L+1}^\Omega} a(v - I_L^\Omega v, v - I_L^\Omega v) \leq \frac{1}{\lambda_{L+1}^\Omega} a(v, v). \tag{18}$$

When $L = 1$ we obtain the usual Poincaré inequality since it can be verified that $\lambda_2^\Omega = O(\mathrm{diam}(\Omega)^{-2})$ where $\mathrm{diam}(\Omega)$ is the diameter of Ω (cf. [14]).

We note that $\{\omega_i\}_{y_i \in \mathcal{T}^H}$ is a covering of Ω. Let $\{\chi_i\}_{i=1}^{N_c}$ be a partition of unity subordinated to the covering $\{\omega_i\}$ such that $\chi_i \in V^h(D)$ and $|\nabla \chi_i| \leq \frac{1}{H}$, $i = 1, \ldots, N_c$. Define the set of coarse basis functions

$$\Phi_{i,\ell} = I^h(\chi_i \psi_\ell^{\omega_i}) \quad \text{for } 1 \leq i \leq N_c \text{ and } 1 \leq \ell \leq L_i \tag{19}$$

where I^h is the fine-scale nodal value interpolation and L_i is an integer number for each $i = 1, \ldots, N_c$. Denote by V_0 the *local spectral multiscale* space

$$V_0 = \mathrm{span}\{\Phi_{i,\ell} : 1 \leq i \leq N_c \text{ and } 1 \leq \ell \leq L_i\}. \tag{20}$$

It is easy to see that the new basis functions $\Phi_{i,\ell}$ defined in (19) are linearly independent and $\dim(V_0) = \sum_{i=1}^{N_c} L_i$. Define also the coarse interpolation $I_0 : V^h(D) \to V_0$ by

$$I_0 v = \sum_{i=1}^{N_c} \sum_{\ell=1}^{L_i} \left(\int_{\omega_i} \kappa v \psi_\ell^{\omega_i} \right) I^h(\chi_i \psi_\ell^{\omega_i}) = \sum_{i=1}^{N_c} I^h \left((I_{L_i}^{\omega_i} v) \chi_i \right), \tag{21}$$

where I^h is the fine-scale nodal value interpolation and $I_{L_i}^{\omega_i}$ is defined in (17). Note that we have

$$v - I_0 v = \sum_{i=1}^{N_c} I^h \left(\chi_i (v - I_{L_i}^{\omega_i} v) \right).$$

We will use the following lemma.

Proposition 1 *For any $z \in \mathbb{P}^3(K)$ (the space of polynomials of degree 3 or less) we have that*

$$\int_K \kappa |I^h z|^2 \preceq \int_K \kappa |z|^2 \tag{22}$$

and

$$\int_K \kappa |\nabla I^h z|^2 \preceq \int_K \kappa |\nabla z|^2. \tag{23}$$

The proof of this proposition is given in Appendix A.

We have the following weighted L^2 approximation and weighted H^1 stability properties.

Lemma 2 *For all coarse element K we have*

$$\int_K \kappa (v - I_0 v)^2 \preceq \frac{1}{\lambda_{K,L+1}} \int_{\omega_K} \kappa |\nabla v|^2 \tag{24}$$

$$\int_K \kappa |\nabla I_0 v|^2 \preceq \max\{1, \frac{1}{H^2 \lambda_{K,L+1}}\} \int_{\omega_K} \kappa |\nabla v|^2 \tag{25}$$

where $\lambda_{K,L+1} = \min_{y_i \in K} \lambda_{L_i+1}^{\omega_i}$ and ω_K is the union of the elements that share common edge with K defined in (10).

Proof. First we prove (24). Using (22) and the fact that $\chi_i \leq 1$ we have

$$\begin{aligned}
\int_K \kappa (v - I_0 v)^2 &\preceq \sum_{y_i \in K} \int_K \kappa I^h (\chi_i (v - I_{L_i}^{\omega_i} v)^2 && (26)\\
&\preceq \sum_{y_i \in K} \int_K \kappa (\chi_i (v - I_{L_i}^{\omega_i} v))^2 && (27)\\
&\preceq \sum_{y_i \in K} \int_{\omega_i} \kappa (v - I_{L_i}^{\omega_i} v)^2 && (28)
\end{aligned}$$

and using (18) with $\Omega = \omega_i$ to estimate the last term above, we obtain

$$\int_K \kappa(v - I_0 v)^2 \preceq \sum_{y_i \in K} \frac{1}{\lambda_{L+1}^{\omega_i}} \int_{\omega_i} \kappa |\nabla v|^2 \tag{29}$$

$$\preceq \max_{y_i \in K} \frac{1}{\lambda_{L+1}^{\omega_i}} \int_{\omega_K} \kappa |\nabla v|^2. \tag{30}$$

To prove the stability (25) we note that in K

$$\sum_{y_i \in K} \nabla \chi_i = 0,$$

and then we can write $\nabla \chi_j = -\sum_{y_i \in K \setminus \{y_j\}} \nabla \chi_i$. We obtain,

$$\nabla \sum_{y_i \in K} (I_{L_i}^{\omega_i} v) \chi_i = \sum_{y_i \in K} \nabla \chi_i (I_{L_i}^{\omega_i} v) + \sum_{y_i \in K} \chi_i \nabla (I_{L_i}^{\omega_i} v) \tag{31}$$

$$= \sum_{y_i \in K \setminus \{y_j\}} (I_{L_i}^{\omega_i} v - I_{L_j}^{\omega_j} v) \nabla \chi_i + \sum_{y_i \in K} \chi_i \nabla (I_{L_i}^{\omega_i} v) \tag{32}$$

which gives the following bound valid on K,

$$|\nabla \sum_{y_i \in K} (I_{L_i}^{\omega_i} v) \chi_i|^2 \preceq \frac{1}{H^2} \sum_{y_i \in K \setminus \{y_j\}} (I_{L_i}^{\omega_i} v - I_{L_j}^{\omega_j} v)^2 + \sum_{y_i \in K} |\nabla (I_{L_i}^{\omega_i} v)|^2. \tag{33}$$

Since $\sum_{y_i \in K} (I_{L_i}^{\omega_i} v) \chi_i \in \mathbb{P}^3(K)$ we can use (23) and (33) to get

$$\int_K \kappa |\nabla I_0 v|^2 = \int_K \kappa |\nabla I^h (\sum_{y_i \in K} (I_{L_i}^{\omega_i} v) \chi_i)|^2 \tag{34}$$

$$\preceq \int_K \kappa |\nabla \sum_{y_i \in K} (I_{L_i}^{\omega_i} v) \chi_i|^2 \tag{35}$$

$$\preceq \sum_{y_i \in K} \frac{1}{H^2} \int_K \kappa (I_{L_i}^{\omega_i} v - I_{L_j}^{\omega_j} v)^2 + \sum_{y_i \in K} \int_K \kappa |\nabla (I_{L_i}^{\omega_i} v)|^2. \tag{36}$$

To bound the first term above we use (18) with $\Omega = \omega_i$ as follows,

$$\int_K \kappa (I_{L_i}^{\omega_i} v - I_{L_j}^{\omega_j} v)^2 \preceq \int_{\omega_i} \kappa (v - I_{L_i}^{\omega_i} v)^2 + \int_{\omega_j} \kappa (v - I_{L_i}^{\omega_i} v)^2 \tag{37}$$

$$\preceq \frac{1}{\lambda_{L+1}^{\omega_i}} \int_{\omega_i} \kappa |\nabla v|^2 + \frac{1}{\lambda_{L+1}^{\omega_j}} \int_{\omega_j} \kappa |\nabla v|^2 \tag{38}$$

$$\preceq \frac{1}{\lambda_{K,L+1}} \int_{\omega_K} \kappa |\nabla v|^2. \tag{39}$$

The second term in (36) is estimated using (15) and the orthogonality of the eigenvectors in the A^{ω_i} inner product

$$\int_K \kappa |\nabla (I_{L_i}^{\omega_i} v)|^2 \leq \int_{\omega_i} \kappa |\nabla (I_{L_i}^{\omega_i} v)|^2 \leq \int_{\omega_i} \kappa |\nabla v|^2 \leq \int_{\omega_K} \kappa |\nabla v|^2. \tag{40}$$

By combining (39), (40) and (36) we obtain (25). ∎

Remark 3 *Assume that* $\kappa(x) = 1$ *for all* $x \in D$ *and* $L_i = 1$ *for all* $i = 1, \ldots, N_c$. *Then (24) becomes*

$$\int_K \kappa(v - I_0 v)^2 \preceq H^2 \int_{\omega_K} \kappa |\nabla v|^2$$

and (25)

$$\int_K \kappa |\nabla I_0 v|^2 \preceq \int_{\omega_K} \kappa |\nabla v|^2$$

since $\lambda_{K,L+1} = \max_{y_i \in K} \lambda^{\omega_i}_{L_i+1} \asymp H^{-2}$.

5 Domain decomposition with the local spectral multiscale space

In this section, we show that if the coarse space is the local spectral multiscale space as introduced in (20), then the condition number of the preconditioned matrix is independent of the contrast.

5.1 Analysis

In this section we estimate the condition number of the preconditioned operator $B^{-1}A$ with B^{-1} defined in (7) using the coarse space V_0 in (20). From the abstract domain decomposition theory we only need to prove the stable decomposition property; see [18, 23].

Lemma 4 *For all* $v \in V^h$, *there exists a decomposition* $v = \sum_{i=0}^{N} v_i$, *with* $v_i \in V^i = V_0^h(D_i')$, $i = 1, 2, \ldots, N$, $v_0 \in V_0$, *such that*

$$a(v_0, v_0) + \sum_{i=1}^{N} a(v_i, v_i) \preceq C_0^2 a(v, v)$$

with $C_0^2 \preceq \max\{1 + \frac{1}{\delta^2 \lambda_{L+1}}, 1 + \frac{1}{H^2 \lambda_{L+1}}\}$ *where* $\lambda_{L+1} = \min\limits_{1 \le i \le N_c} \lambda^{\omega_i}_{L_i+1}$.

Proof. Define $v_0 := I_0 v_h$ where I_0 is a coarse interpolation defined in (21) and

$$v_i = I^h(\xi_i(v - v_0)).$$

Here $\{\xi_i\}$ is a partition of unity subordinated to the overlapping partition $\{D_i'\}$ such that $\xi_i \in V^h$ and $|\nabla \xi_i| \le \frac{1}{\delta}$, $i = 1, \ldots, N$. First we bound the energy of

the local functions v_i, $i = 1, \ldots, N$.

$$\begin{aligned} a(v_i, v_i) &= \int_{D_i'} \kappa |\nabla I^h(\xi_i(v - v_0))|^2 \\ &\preceq \int_{D_i'} \kappa |\nabla(\xi_i(v - v_0))|^2 \\ &\preceq \int_{D_i'} \kappa \xi_i^2 |\nabla(v - v_0)|^2 + \int_{D_i'} \kappa |\nabla \xi_i|^2 |v - v_0|^2 \\ &\leq \int_{D_i'} \kappa |\nabla(v - v_0)|^2 + \frac{1}{\delta^2} \int_{D_i' \setminus \overline{D_i}} \kappa |v - v_0|^2 \\ &\preceq \int_{D_i'} \kappa |\nabla v|^2 + \int_{D_i'} \kappa |\nabla v_0|^2 + \frac{1}{\delta^2} \int_{D_i' \setminus \overline{D_i}} \kappa |v - v_0|^2. \end{aligned} \tag{41}$$

Now we bound the last two terms of (41).

The second term in (41) can be bounded using (25) of Lemma 2 as follows

$$\int_{D_i'} \kappa |\nabla v_0|^2 \leq \sum_{\overline{K} \cap \overline{D}_i \neq \emptyset} \int_K \kappa |\nabla v_0|^2 \preceq \max\{1, \frac{1}{H^2 \lambda_{L+1}}\} \sum_{K \cap \overline{D}_i \neq \emptyset} \int_{\omega_K} \kappa |\nabla v|^2.$$

To bound the third term of (41) observe that, using (24) in Lemma 2

$$\begin{aligned} \frac{1}{\delta^2} \int_{D_i' \setminus \overline{D_i}} \kappa |v - v_0|^2 &\preceq \frac{1}{\delta^2} \sum_{K \cap \overline{D}_i \neq \emptyset} \int_K \kappa |v - v_0|^2 \\ &\preceq \frac{1}{\lambda_{L+1} \delta^2} \sum_{K \cap \overline{D}_i \neq \emptyset} \int_{\omega_K} \kappa |\nabla v|^2. \end{aligned} \tag{42}$$

The bound for the energy $a(v_0, v_0)$ follows from (25) of Lemma 2,

$$a(v_0, v_0) \leq \max\{1, \frac{1}{H^2 \lambda_{L+1}}\} a(v, v).$$

■

We have the following bound for the condition number of the preconditioned operator.

Corollary 5 *Under the assumptions of Lemma 4, the condition number of the preconditioned operator $B^{-1}A$ with B^{-1} defined in (7) is of order*

$$cond(B^{-1}A) \preceq C_0^2 \preceq \max\{1 + \frac{1}{\delta^2 \lambda_{L+1}}, 1 + \frac{1}{H^2 \lambda_{L+1}}\}$$

where $\lambda_{L+1} = \min_{1 \leq i \leq N_c} \lambda_{L_i+1}^{\omega_i}$.

We note that the eigenvalues of the local problem scale as H^{-2}. This can be easily shown by mapping the local eigenvalue problem corresponding to ω_i to the union of reference elements, say $\widehat{\omega}_i$. In this case we have that $H^2\lambda_i \asymp \hat{\lambda}_\ell^{\widehat{\omega}_i}$ and if we use $\delta \asymp H$ the bound for C_0 in Lemma 4 can be seen to be independent of the parameter H of the coarse triangulation. Thus, we have the following result.

Corollary 6 *Under the assumptions of Lemma 4 the condition number of the preconditioned operator $B^{-1}A$ with B^{-1} defined in (7) is*

$$cond(B^{-1}A) \preceq C(1 + \frac{H^2}{\delta^2})$$

where C is independent of the contrast and the mesh size.

5.2 Numerical results

In this section, we present representative numerical results for the additive preconditioner (7) with the local spectral multiscale coarse space defined in (20). We show numerically that the condition number of the resulting preconditioned system is independent of the contrast as our theory shows. We take $D = [0,1] \times [0,1]$ that is divided into 10×10 equal square subdomains. Inside each subdomain we use a fine-scale triangulation where triangular elements constructed from 10×10 squares are used. We use the coefficient in Figure 3 that corresponds to a coefficient with background one and (7×7) circular inclusions with high coefficient η inside each inclusion. We run the preconditioned conjugate gradient until the ℓ_2 norm of the initial residual is reduced by a factor of 10^{-10}.

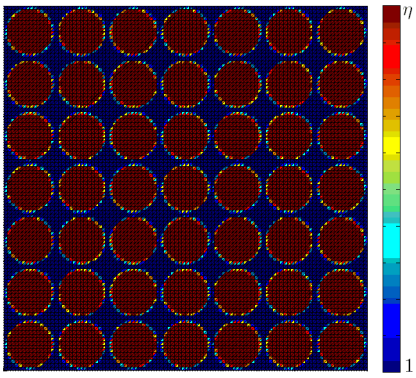

Figure 3: Coefficient. Red designates the regions where the coefficient is η and blue designates the regions where the coefficient is 1. The numerical results are presented in Table 1.

η	One level	Linear	MS	EMF	LSM_1	LSM_2
10^4	65(1.6e+3)	81(3.8e+3)	68(2.1e+3)	52(3.8e+2)	53(54.29)	46(32.04)
10^5	70(1.5e+4)	88(3.8e+4)	73(2.1e+4)	60(3.8e+3)	41(56.25)	40(32.73)
10^6	78(1.5e+5)	111(3.8e+5)	91(2.1e+5)	68(3.8e+4)	40(56.53)	37(33.40)
10^7	93(1.5e+6)	141(3.8e+6)	112(2.1e+6)	76(3.8e+5)	37(56.52)	36(41.35)
10^8	103(1.5e+7)	156(3.8e+7)	129(2.1e+7)	86(3.8e+6)	37(56.42)	33(42.47)
10^9	111(1.5e+8)	175(3.8e+9)	143(2.1e+8)	73(2.3e+7)	30(54.88)	30(42.59)

Table 1: Number of iterations until convergence of the PCG and condition number for different values of the contrast η with the coefficient depicted in Figure 3. We set the tolerance to 1e-10. Here $H = 1/10$ with $h = 1/100$. The classical (one basis per node) coarse problems size is 81×81. The new coarse problem is of size 321×321.

To test our new method we implemented two level additive preconditioner with three of the classical coarse spaces: P^1-linear functions (Linear), multiscale functions with linear boundary condition (MS) and energy minimizing functions (EMF). The definition of the new local spectral multiscale coarse space V_0 in (20) depends on the choice of a partition of unity. In the first numerical experiments we will use two partition of unity functions: P^1 bilinear functions (LSM_1) and usual multiscale functions (see [19]) with linear boundary conditions (LSM_2). In next sections, we will discuss other choices of the partition of unity. In Table 1 we set

$$L_i = L = \max_{\lambda_\ell \leq 2} \ell \tag{43}$$

for all $i = 1, \ldots, N_c$. We note that $L_i \leq 4$ for all $i = 1, \ldots, N_c$ in this case.

In Table 1 we present the number of iterations until convergence and in parenthesis the conjugate gradient estimate for the condition number of the preconditioned operator for the methods mentioned above. The results show an agreement with our theory. We observe that for the classical coarse spaces the number of iterations and the condition number depend on the contrast (η) while for the new coarse spaces (last two columns) the number of iterations and the condition number remains bounded as the contrast increases. The dimension of the classical coarse matrix is 81×81 and the dimension of the new coarse problem is 321×321. This is even smaller than the dimension of one local problem 400×400. In Section 7 we will introduce a smaller local spectral coarse problem with less basis functions and with the condition number still independent of the contrast of the media.

6 The least energy basis approach

6.1 Energy minimizing partition of unity

In previous section, we used general partition of unity functions. One can use the partition of unity functions $\{\chi_i\}_{i=1}^{N_c}$ that provide the least energy. This can

be accomplished by solving

$$\min \sum_{i=1}^{N_c} \sum_{\ell=1}^{L_i} \int_{\omega_i} \kappa |\nabla \Phi_{i,\ell}|^2 = \min \sum_{i=1}^{N_c} \sum_{\ell=1}^{L_i} \int_{\omega_i} \kappa |\nabla (\chi_i \psi_\ell^{\omega_i})|^2 \tag{44}$$

where the local spectral multiscale basis functions $\Phi_{i,\ell}$ are defined in (19) and the minimum is taken over all partition of unity functions $\{\chi_i\}_{i=1}^{N_c}$ subordinated to the covering $\{\omega_i\}_{i=1}^{N_c}$ of D. In [24], the authors considered energy minimizing partition of unity basis for $\kappa(x)$. This is the same if we take one constant unity eigenfunction in our formulation. One can solve (44) following the similar procedure as discussed in [24].

The numerical solution of the energy minimizing problem (44) is computationally intensive and requires computing a global problem. One can use instead multiscale basis functions that share similarities with energy minizing basis functions. In particular, they reduce the energies of the basis functions. In this section, we consider the multiscale framework that can compute basis functions with less energy by solving one local problem per coarse block.

We define the *local spectral multiscale basis functions with reduced energy* $\widetilde{\Phi}_{i,\ell}$ as the $\kappa-$harmonic extension of $\Phi_{i,\ell}$ in each coarse block, that is, for each coarse element K and $1 \leq \ell \leq L_i$ with $1 \leq i \leq N_c$ we have

$$\begin{aligned} \int_K \kappa \nabla \widetilde{\Phi}_{i,\ell} \nabla z &= 0 \quad \text{for all } z \in V_0^h(K), \\ \widetilde{\Phi}_{i,\ell} &= \Phi_{i,\ell} \quad \text{on } \partial K. \end{aligned} \tag{45}$$

We define *local spectral multiscale coarse space with reduced energy* by

$$V_0 = \text{span}\{\widetilde{\Phi}_i\}_{i=1}^{N_c}. \tag{46}$$

Next, we will present numerical results with these basis functions. Furthermore, the functions (44) or (45) will be used to reduce the dimension of the coarse space.

6.2 Numerical results

In this section, we present numerical results using *local spectral coarse space* V_0 *with reduced energy* defined in (45) and (46). In the next section, these basis functions will be used to reduce the dimension of the coarse space by replacing the basis functions with bounded, independent of the contrast, energies with multiscale finite element basis functions. They can also be replaced by energy minimizing basis functions as defined e.g., in [24, 16]. Our numerical results show that the number of iterations required by domain decomposition methods is independent of contrast and smaller compared when using *local spectral coarse space* V_0 defined in (20). We consider $D = [0,1] \times [0,1]$ that is divided into 8×8 equal square subdomains with a fine scale triangular elements constructed

from 10×10 squares. We use the coefficient in Figure 4 that corresponds to the case with the background conductivity one and broken channels with high conductivity η. Similar results hold for the coefficient in Section 5.2. We run the preconditioned conjugate gradient until the ℓ_2 norm of the initial residual is reduced by a factor of 10^{-10}.

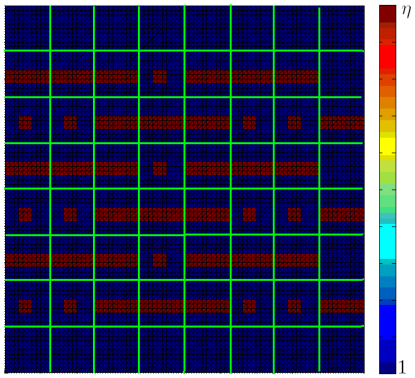

Figure 4: Coefficient and coarse mesh. Red designates the regions where the coefficient is η and blue designates the regions where the coefficient is 1. The numerical results are presented in Table 2.

η	Linear	MS	EMF	LSM_1	LSM_2	LSM-RE
10^4	92(3.5e+3)	77(2.3e+3)	57(364.12)	33(8.54)	32(8.40)	29(8.25)
10^5	109(3.4e+4)	93(2.2e+4)	58(404.85)	34(8.56)	34(8.42)	28(8.27)
10^6	124(3.4e+5)	107(2.3e+5)	67(409.46)	35(8.56)	34(8.42)	29(8.27)
10^7	144(3.4e+6)	137(2.3e+6)	77(409.93)	36(8.56)	35(8.42)	31(8.27)
10^8	163(3.4e+7)	159(2.3e+7)	82(409.97)	37(8.56)	36(8.41)	32(8.27)
10^9	206(3.4e+8)	198(2.3e+8)	86(409.98)	37(8.56)	38(8.39)	32(8.27)

Table 2: Number of iterations until convergence of the PCG and condition number for different values of the contrast η with the coefficient in Figure 4. We set the tolerance to 1e-10. Here $H = 1/8$ with $h = 1/80$. The classical coarse space is of dimension 49×49 and the dimension of the new coarse space is 126×126.

As before we compare domain decomposition methods with spectral coarse spaces and domain decomposition methods with classical spaces: P^1-linear functions (Linear), multiscale functions with linear boundary condition (MS), energy minimizing functions (EMF). We also use two partition of unity functions: P^1 bilinear functions (LSM_1) and usual multiscale functions with linear boundary conditions (LSM_2). The local spectral multiscale coarse space with reduced energy (LSM-RE) uses the space V_0 defined in (46). The number of eigenvalues in each node is computed as before, see (43).

In Table 2 we present the number of iterations until convergence and in the parenthesis the conjugate gradient estimate for the condition number of the preconditioned operator. We observe that for the new coarse space (last three columns) the number of iterations and the condition number remain bounded as the contrast increases. We see that the domain decomposition methods with local spectral coarse space with reduced energy (defined in (46)) performs slightly better than the local spectral coarse space (defined in (20)).

Next, we repeat the previous experiment with the coefficient in Figure 5. The results are presented in Table 3. For these coefficients we use non-horizontal broken channels. We observe similar results as in the previous example. In this case, domain decomposition methods with the local spectral multiscale coarse space with reduced energy perform better than domain decomposition methods with local spectral multiscale space.

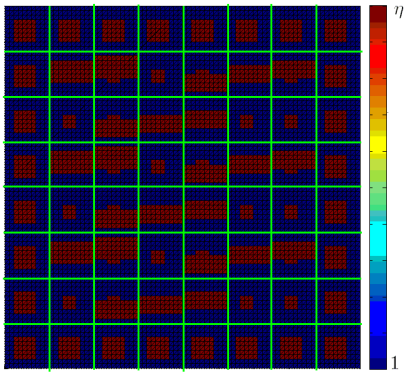

Figure 5: Coefficient and coarse mesh. Red designates the regions where the coefficient is η and blue designates the regions where the coefficient is 1. The numerical results are presented in Table 3.

η	Linear	MS	EMF	LSM_1	LSM_2	LSM-RE
10^4	114(6.21e+3)	96(2.38e+3)	62(2.45e+2)	41(1.32e+1)	33(6.58)	27(6.16)
10^5	138(6.20e+4)	125(2.37e+4)	64(2.71e+2)	42(1.32e+1)	33(6.58)	28(6.16)
10^6	162(6.20e+5)	151(2.37e+5)	64(2.74e+2)	43(1.32e+1)	33(6.58)	31(6.16)
10^7	184(6.20e+6)	173(2.37e+6)	74(2.75e+2)	44(1.32e+1)	34(6.58)	27(6.16)
10^8	209(6.20e+7)	219(2.37e+7)	81(2.75e+2)	45(1.32e+1)	36(6.58)	28(6.16)
10^9	281(6.20e+8)	249(2.37e+8)	87(2.75e+2)	48(1.32e+1)	38(6.57)	30(6.16)

Table 3: Number of iterations until convergence of the PCG and condition number for different values of the contrast η with the coefficient in Figure 5. We set the tolerance to 1e-10. Here $H = 1/8$ with $h = 1/80$. The classical coarse space is of dimension 49×49 and the dimension of the new coarse space is 166×166.

We note that in both cases, several eigenfunctions per node are used for constructing the coarse spaces. As a result, the coarse dimensional problems

are 126×126 and 166×166 in the examples corresponding to Tables 2 and 3, respectively. In the next section, we discuss how one can reduce the dimension of the coarse space by using local spectral multiscale space with reduced energy.

7 Reducing the dimension of the coarse space

7.1 Reduced local spectral multiscale

As the high-contrast eigenvalue problem suggests that one can have a large number of basis functions if the number of separate high-contrast regions is large. This will result to a large dimensional coarse space. On the other hand, it is known that for problems when high contrast inclusions are separated and away from the boundaries of coarse-grid blocks, one can use multiscale finite element basis functions for constructing the coarse space. In this section, we propose an approach that allows reducing the dimension of the coarse space. The analysis of this approach is a subject of the future research.

Our motivation for the reduction stems from the fact that when high-contrast inclusions are isolated and away from the boundaries of coarse-grid blocks, the energies of the basis functions are bounded unlike the energies of the basis functions corresponding to channels. For this reason, we perform local singular value decomposition and isolate the basis functions that represent high-conductivity channels from basis functions that represent the inclusions with bounded energy. The approach is as follows. Given a coarse mesh node y_i we consider the space spanned by all the coarse basis functions associated to this node. Here, we take local spectral coarse space with reduced energy as defined in (46) with multiscale or energy minimizing partition of unity basis functions defined in (44). Then divide this space according to the energy, keeping the part of the space with higher energy. More precisely, consider the L_i basis functions associated to this node, that is

$$\Phi_{i,\ell}, \text{ with } 1 \leq \ell \leq L_i$$

and define the matrix

$$R_0^{iT} = [\Phi_{i,1}, \ldots, \Phi_{i,L_i}].$$

We have that the coarse space spanned by multiscale basis functions (see (20)) can be written as $V_0 = \text{span}_{1 \leq i \leq N_c} R_0^{iT}$. We define the local coarse matrix of dimension $L_i \times L_i$ by

$$A_0^i = R_0^{iT} A R_0^i.$$

In the case of V_0 defined by (46) the basis functions $\Phi_{i,1}$ are usual multiscale basis functions with linear boundary conditions. We write the eigenvalue decomposition of this symmetric matrix as

$$A_0^i = Q_0^{Ti} D_0^i Q_0^i, \quad Q_0^i = [q_{i,1}, \ldots, q_{i,L_i}] \tag{47}$$

where the matrix Q_0^i is an orthogonal matrix and $D_0^i = \text{diag}(\mu_1, \ldots, \mu_{L_i})$ with

$$\mu_1 \leq \ldots \leq \mu_{L_i}.$$

The idea is to keep only the part of span$\{R_0^{iT}\}$ associated with larger energy. To do this we remove the first M_i eigenvectors in (47) that have bounded energies independent of the contrast (see Section 7.2 for numerical implementation). In case of interior high-contrast inclusions and channels, M_i can be chosen as the number of small, asymptotically vanishing, eigenvalues corresponding to the zero Dirichlet local high-contrast eigenvalue problem. Define the matrix of eigenvectors of larger energy by

$$\widehat{Q}_0^i = [0, \ldots, 0, q_{i,M_i+1} \ldots, q_{i,L_i}].$$

The new basis functions associated to the coarse mesh node y_i will be given by the columns of the matrix $R_0^i \widehat{Q}_0^i$ and the multiscale basis function $\Phi_{1,i}$ (or energy minimizing basis functions as defined in [16, 24]). We define the new reduced local spectral multiscale space

$$V_0 = \text{span}\{\Phi_{i,1}, R_0^i \widehat{Q}_0^i\}_{i=1}^{N_c}. \tag{48}$$

Note that one can determine the number of basis functions associated with interior inclusions by solving zero Dirichlet eigenvalue problem instead of zero Neumann problem. However, to identify the eigenvectors that represent channels is not easy. Many eigenvectors have components in the channels and they all have the same energy. By using local spectral multiscale coarse space with reduced energy, we can identify the basis corresponding to inclusions simply by identifying the elements of the span of these basis functions with bounded energies. This is the main idea of the presentation above.

If isolated inclusions intersect the boundaries, multiscale finite element basis functions with linear boundary conditions can give large (contrast dependent) energies for such isolated inclusions. In [15], the authors construct multiscale basis functions with bounded energies for isolated high-contrast inclusions intersecting the boundary. These basis functions are constructed using one dimensional solutions as boundary conditions. In [16], the authors show that one can also use energy minimizing concept to obtain basis functions with bounded energies for the case of high-contrast isolated inclusions intersecting the boundary of a coarse block. In our formulation, local spectral basis functions given by (44), instead of (45), can be used to reduce the coarse space for the case with isolated inclusions intersecting the boundary of a coarse block. In this case the basis functions with bounded energies will be replaced by energy minimizing basis functions as defined in [16].

7.2 Numerical experiments

In this section, we present numerical results using the reduced coarse space as defined in (48). We show numerically that the condition number of the resulting preconditioned system is independent of the contrast. In this case, we again consider $D = [0, 1] \times [0, 1]$ that is divided into equal 8×8 square subdomains with fine-scale triangular elements constructed from 10×10 squares. We use the coefficient shown in Figure 6 that has background one conductivity with three

high conductivity channels and several square inclusions with high conductivity. Here we only consider the case of isolated interior inclusions and channels. We run the preconditioned conjugate gradient until the ℓ_2 norm of the initial residual is reduced by a factor of 10^{-10}.

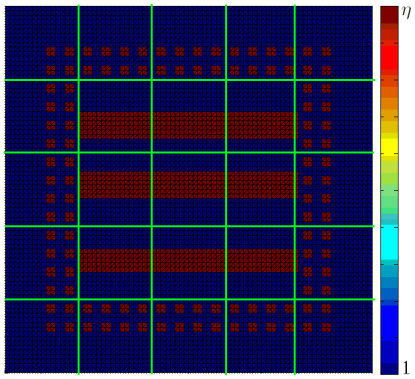

Figure 6: Coefficient and coarse mesh. Red designates the regions where the coefficient is η and blue designates the regions where the coefficient is 1. The numerical results are presented in Table 4.

η	MS	EMF	LSM_1	LSM_2	RLSM
10^4	38(1.97e+3)	34(3.30e+2)	35(3.85e+1)	27(6.26)	33(1.55e+1)
10^5	44(1.97e+4)	36(3.77e+2)	36(3.79e+1)	28(6.19)	32(1.59e+1)
10^6	48(1.97e+5)	44(3.83e+2)	40(3.88e+1)	30(5.82)	32(1.60e+1)
10^7	54(1.97e+6)	44(3.83e+2)	42(3.90e+1)	31(6.03)	32(1.60e+1)
10^8	89(1.97e+7)	47(3.83e+2)	43(3.91e+1)	31(6.24)	34(1.60e+1)
10^9	103(1.97e+8)	48(3.83e+2)	44(3.90e+1)	31(6.26)	38(1.60e+1)

Table 4: Number of iterations until convergence of the PCG and condition number for different values of the contrast η with the coefficient depicted in Figure 6. We set the tolerance to 1e-10. Here $H = 1/4$ with $h = 1/80$. The classical coarse problem is of dimension 16×16, the dimension of the LSM space is 232×232 and the dimension of the reduced space RLSM is 36×36.

In Table 4 we present the number of iterations until convergence and in parenthesis the conjugate gradient estimate for the condition number of the preconditioned operator. In our simulations we define L_i as before, see (43), and remove the eigenvectors of the local problem (47) with small energies. In particular, in the presence of channels (that can be, in general, identified by comparing Dirichlet and Neumann high-contrast eigenvalue problems) we eliminate the eigenfunctions with less than 5% of the total energy. These eigenfunctions represent interior high-contrast inclusions. If the media consist of only interior inclusions (that can be identified by using Dirichlet high-contrast eigenvalue problem), we simply use multiscale basis functions. In our current

simulations, we do not perform any additional dimension reduction for those high-contrast inclusions that intersect the boundary of a coarse grid. In Table 4, LSM_1 and LSM_2 refer to domain decomposition methods with local spectral multiscale coarse space as defined in (20), LSM-RE refers to domain decomposition methods with local spectral multiscale coarse space as defined in (46), and RLSM refers to domain decomposition methods with local spectral multiscale coarse space as defined in (48). We observe that for local spectral coarse spaces LSM_1, LSM_2 and RLSM the number of iterations and condition number remains bounded as the contrast increases. This is also true for the energy minimizing functions coarse space (EMF). The computations corresponding to the reduced energy space LSM-RE are affected by the high condition number of the coarse problem due to very large coarse space. This issue is not present in the reduced space RLSM. The size of the classic coarse space (one basis per node) is 16×16 while the size of the LSM space is 232×232. The size of the reduced coarse space is 36×36. We see a significant reduction in the size of the coarse problem with condition number still being independent of the contrast of the coefficient. In future, we plan to investigate the dimension reduction for the coarse space in the presence of isolated inclusions intersecting the boundary of a coarse block using the energy minimizing functions defined in (44) (see the discussion at the end of Section 7.1).

8 Conclusions

In this paper, we study domain decomposition preconditioners for multiscale elliptic problems in high contrast media. We assume that each coarse-grid block can have large variations in the media properties. We construct domain decomposition preconditioners such that the condition number of the preconditioned system is independent of media contrast for general multiscale high-contrast problems. The central part of this work is the construction of coarse spaces that satisfy weighted L^2 stability requirement with stability constant independent of the contrast. The latter is needed to guarantee that the condition number of domain decomposition methods is independent of the contrast. The weighted L^2 stability estimate suggests the use of weighted eigenvalue problems for the construction of the coarse space. A main observation is that the eigenvalues of this spectral problem controls the condition number. In the presence of high-contrast inclusions, there are small, asymptotically vanishing, eigenvalues. These eigenvalues decrease as we increase the contrast. We propose the coarse space that includes the eigenfunctions corresponding to these small, asymptotically vanishing, eigenvalues. We prove that domain decomposition preconditioners with this coarse space have the condition number independent of the contrast. In general, the coarse space can be large if there are many isolated inclusions. We propose approaches to reduce the dimension of the coarse space. Numerical results are presented. We compare the proposed methods with domain decomposition methods where multiscale finite element basis or energy minimizing basis functions are used in constructing coarse spaces. We

show that the number of iterations is smaller with proposed methods and they remain bounded as the contrast increases.

9 Acknowledgments

This work is partially supported by Award Number KUS-C1-016-04, made by King Abdullah University of Science and Technology (KAUST). YE's research is partially supported by NSF and DOE.

A Proof of Proposition 1

First we prove (22). Let $e \subset K$ be an fine scale element. We have

$$\int_e |I^h z|^2 \preceq \sum_{x_k \in e} z(x_k)^2 \int_e |\phi_k|^2 \tag{49}$$

$$\preceq \|z\|_\infty^2 h^2 \preceq \|z\|_{L^2(e)}^2 = \int_e z^2 \tag{50}$$

where we have used an inverse estimate $\|z\|_\infty \preceq h^{-1}\|z\|_{L^2(e)}$ that is valid for all third degree polynomials z on e; see [7, Lemma 4.5.3]. Multiplying by $\kappa(x) = \kappa_e$ and summing over all elements in $e \subset K$ we get (22).

Analogously given any constant c if we define the second degree polynomial $\hat{z} = z - c$ we have

$$\int_e |\nabla I^h \hat{z}|^2 \preceq \sum_{x_k \in e} \hat{z}(x_k)^2 \int_e |\nabla \phi_k|^2 \tag{51}$$

$$\preceq \|\hat{z}\|_\infty^2 \preceq \|\hat{z}\|_{H^1(e)}^2 \tag{52}$$

where we have used an inverse estimate $\|\hat{z}\|_\infty \preceq \|\hat{z}\|_{H^1(e)}$ that is valid for all third degree polynomials $\hat{z}$ on e, [7, Lemma 4.5.3]. Now by choosing c as the mean value of z on the element e, we can apply a Poincaré inequality to obtain

$$\int_e |\nabla I^h z|^2 \preceq \|z - c\|_{H^1(e)}^2 \preceq \int_e |\nabla z|^2. \tag{53}$$

Multiplying by κ_e and summing over all elements in K we get (23).

References

[1] J. E. Aarnes, *On the use of a mixed multiscale finite element method for greater flexibility and increased speed or improved accuracy in reservoir simulation*, SIAM MMS, 2 (2004), pp. 421–439.

[2] J. E. Aarnes, Y. Efendiev, and L. Jiang, *Analysis of Multiscale Finite Element Methods using Global Information For Two-Phase Flow Simulations*, SIAM MMS, 2008.

[3] J. Aarnes and T. Hou, *Multiscale domain decomposition methods for elliptic problems with high aspect ratios*, Acta Math. Appl. Sin. Engl. Ser., 18(1):63–76, 2002.

[4] J. E. Aarnes, S. Krogstad, and K.-A. Lie, *A hierarchical multiscale method for two-phase flow based upon mixed finite elements and nonuniform grids*, Multiscale Model. Simul. 5(2) (2006), pp. 337–363.

[5] T. Arbogast, *Implementation of a locally conservative numerical subgrid upscaling scheme for two-phase Darcy flow*, Comput. Geosci., 6 (2002), pp. 453–481.

[6] T. Arbogast, G. Pencheva, M. F. Wheeler, and I. Yotov, *A multiscale mortar mixed finite element method*, SIAM J. Multiscale Modeling and Simulation, 6(1), 2007, pp. 319-346

[7] S.C. Brenner and L.R. Scott, *The mathematical theory of finite element methods*, vol. 15 of Texts in Applied Mathematics, Springer-Verlag, New York, 1994.

[8] Y. Chen, L.J. Durlofsky, M. Gerritsen, and X.H. Wen, *A coupled local-global upscaling approach for simulating flow in highly heterogeneous formations*, Advances in Water Resources, 26 (2003), pp. 1041–1060.

[9] Z. Chen and T.Y. Hou, *A mixed multiscale finite element method for elliptic problems with oscillating coefficients*, Math. Comp., 72 (2002), pp.541–576 (electronic).

[10] Y. Efendiev, V. Ginting, T. Hou, and R. Ewing, *Accurate multiscale finite element methods for two-phase flow simulations*, J. Comp. Physics, 220 (1), pp. 155-174, 2006.

[11] Y. Efendiev and T. Hou, *Multiscale finite element methods. Theory and applications*. Springer, 2009.

[12] Y. Efendiev, T. Hou, and V. Ginting, *Multiscale finite element methods for nonlinear problems and their applications*, Comm. Math. Sci., 2 (2004), pp. 553–589.

[13] Y. Efendiev, T. Y. Hou, and X. H. Wu, *Convergence of a nonconforming multiscale finite element method*, SIAM J. Num. Anal., 37 (2000), pp. 888–910.

[14] J. Galvis and Y. Efendiev, Domain decomposition preconditioners for multiscale flows in high contrast media, submitted.

[15] I. G. Graham, P. O. Lechner, and R. Scheichl, *Domain decomposition for multiscale PDEs*. Numer. Math., 106(4):589–626, 2007.

[16] I. G. Graham and R. Scheichl, *Robust domain decomposition algorithms for multiscale PDEs*, Numer. Methods Partial Differential Equations, 23(4):859–878, 2007.

[17] I. Lunati and P. Jenny, *Multi-scale finite-volume method for highly heterogeneous porous media with shale layers*, in: Proceedings of the 9th European Conference on the Mathematics of Oil Recovery (ECMOR), Cannes, France, 2004.

[18] T. P. A. Mathew, *Domain decomposition methods for the numerical solution of partial differential equations*, volume 61 of *Lecture Notes in Computational Science and Engineering*. Springer-Verlag, Berlin, 2008.

[19] T.Y. Hou and X.H. Wu, *A multiscale finite element method for elliptic problems in composite materials and porous media*, Journal of Computational Physics, 134 (1997), pp. 169–189.

[20] T. Hughes, G. Feijoo, L. Mazzei, and J. Quincy, *The variational multiscale method - a paradigm for computational mechanics*, Comput. Methods Appl. Mech. Engrg, 166 (1998), pp. 3–24.

[21] P. Jenny, S.H. Lee, and H. Tchelepi, *Multi-scale finite volume method for elliptic problems in subsurface flow simulation*, J. Comput. Phys., 187 (2003), pp. 47–67.

[22] H. Owhadi and L. Zhang, *Metric based up-scaling*, Comm. Pure Appl. Math., Comm. Pure and Applied Math., vol. LX:675-723, 2007.

[23] A. Toselli and O. Widlund. *Domain decomposition methods—algorithms and theory*, volume 34 of *Springer Series in Computational Mathematics*. Springer-Verlag, Berlin, 2005.

[24] J. Xu and L. Zikanov. On an energy minimizing basis for algebraic multigrid methods. *Comput Visual Sci*, 7:121–127, 2004.

[25] J. Xu and J. Zou. Some nonoverlapping domain decomposition methods. *SIAM Rev.*, 40(4):857–914 (electronic), 1998.